

# Pressure sensor realized with polarization-maintaining photonic crystal fiber-based Sagnac interferometer

H. Y. Fu,<sup>1,\*</sup> H. Y. Tam,<sup>1</sup> Li-Yang Shao,<sup>1</sup> Xinyong Dong,<sup>1</sup>  
P. K. A. Wai,<sup>2</sup> C. Lu,<sup>2</sup> and Sunil K. Khijwania<sup>3</sup>

<sup>1</sup>Photonics Research Centre, Department of Electrical Engineering, Hong Kong Polytechnic University, Hung Hom, Kowloon, Hong Kong

<sup>2</sup>Photonics Research Centre, Department of Electronics and Information Engineering, Hong Kong Polytechnic University, Hung Hom, Kowloon, Hong Kong

<sup>3</sup>Department of Physics, Indian Institute of Technology, Guwahati, India

\*Corresponding author: freddy.fu@polyu.edu.hk

Received 3 March 2008; accepted 16 April 2008;  
posted 22 April 2008 (Doc. ID 93390); published 14 May 2008

A novel intrinsic fiber optic pressure sensor realized with a polarization-maintaining photonic crystal fiber (PM-PCF) based Sagnac interferometer is proposed and demonstrated experimentally. A large wavelength-pressure coefficient of 3.42 nm/MPa was measured using a 58.4 cm long PM-PCF as the sensing element. Owing to the inherently low bending loss and thermal dependence of the PM-PCF, the proposed pressure sensor is very compact and exhibits low temperature sensitivity. © 2008 Optical Society of America

OCIS codes: 060.2370, 060.2420, 060.5295.

## 1. Introduction

Optical fiber Sagnac interferometers have been developed for gyroscopes and other sensor applications due to their unique advantages, such as simple design, ease of manufacture, and lower susceptibility to environmental pickup noise in comparison to other types of fiber optic sensors [1,2]. Polarization-maintaining fiber (PMF) is usually used in Sagnac interferometers to introduce optical path difference and cause interference between the two counterpropagating waves in the fiber loop [3–7]. However, conventional PMFs (e.g., Panda and bow-tie PMFs) have a high thermal sensitivity due to the large thermal expansion coefficient difference between boron-doped stress-applying parts and the cladding (normally pure silica). Consequently, conventional PMFs exhibit temperature-sensitive birefringence. Therefore, conventional PMF based Sagnac interferometer sensors exhibit relatively high temperature sensitivity, which is about 1 and 2 orders

of magnitude higher than that of long-period fiber grating (LPG) and fiber Bragg grating (FBG) sensors [3,4]. When they are used for sensing other measurements rather than temperature, such as pressure, the temperature change and fluctuation will cause serious cross-sensitivity effects and would affect the measurement accuracy significantly.

In recent years, polarization-maintaining photonic crystal fiber (PM-PCF) has become commercially available and subsequently has attracted a lot of research interest in investigating its potential in communications and sensing applications [8–10]. PM-PCF possesses very low bending loss due to the large numerical aperture and small-core diameter. This feature is crucial for the realization of practical sensors. It is also significantly less temperature dependent than conventional PMFs due to its pure silica construction without any doped materials in the core or cladding, except with air holes running along the entire length of the fibers. Previous reports showed that the thermal sensitivity of PM-PCF based Sagnac interferometers is 55–164 times smaller than that of conventional

PMF-based ones [11,12]. Temperature-induced cross-sensitivity effects can thus be neglected for sensing applications in which the temperature variation is not too large. Furthermore, owing to the flexible fabrication design of PM-PCF, its birefringence can be much higher than that of conventional PMFs [13]. This helps to reduce the length of the sensing fiber.

Recently, a PM-PCF-based Sagnac interferometer employed as a strain sensor that demonstrated high sensitivity of  $0.23 \text{ pm}/\mu\epsilon$  and measurement range of up to  $32 \text{ em}$  has been reported [9]. A PM-PCF-based pressure sensor with polarimetric detection has also been proposed and demonstrated [10]. Polarimetric sensors are complicated and are generally not preferred in most applications. In this paper, we propose and demonstrate a pressure sensor based on a PM-PCF Sagnac interferometer. The Sagnac loop itself acts as a sensitive pressure sensing element, making it an ideal candidate for pressure sensor. Other reported fiber optic pressure sensors generally required some sort of modification to the fiber to increase their sensitivity [14]. The proposed pressure sensor does not require polarimetric detection and the pressure information is wavelength encoded.

The theoretical analysis for the pressure-induced spectral shift is briefly presented in this paper. Pressure measurement results show a sensing sensitivity of  $3.42 \text{ nm}/\text{MPa}$ , which is achieved by using a  $58.4 \text{ cm}$  PM-PCF-based Sagnac interferometer. The demonstrated measurement range is  $0.3 \text{ MPa}$ , which is limited by the test apparatus available in our laboratory. Important features of the pressure sensor are the low thermal coefficient and the exceptionally low bending loss of the PM-PCF, which permits the fiber to be coiled into a  $5 \text{ mm}$  diameter circle. This allows the realization of a very small pressure sensor.

## 2. Experimental Setup and Operating Principle

Figure 1 shows the experimental setup of our proposed pressure sensor with the PM-PCF based Sagnac interferometer. It includes a conventional 3 dB single-mode fiber coupler and a  $58.4 \text{ cm}$  PM-PCF. The PM-PCF (PM-1550-01, Blaze Photonics) has a beat length of  $<4 \text{ mm}$  at  $1550 \text{ nm}$  and a polarization extinction ratio of  $>30 \text{ dB}$  over  $100 \text{ m}$ . The scanning electron micrograph (SEM) image of the transverse

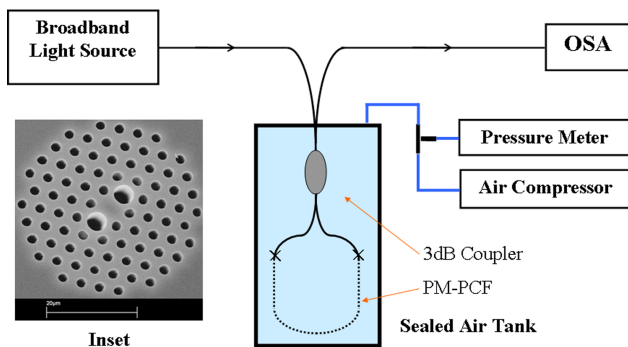


Fig. 1. (Color online) Schematic diagram of the proposed pressure sensor constructed with PM-PCF based Sagnac interferometer.

cross section of the PM-PCF is shown in the inset of Fig. 1. Mode field diameters for the two orthogonal polarization modes are  $3.6$  and  $3.1 \mu\text{m}$ , respectively. The combined loss of the two splicing points is  $\sim 4 \text{ dB}$ . Low splicing loss could be achieved by repeated arc discharges applied over the splicing points to collapse the air holes of the small-core PM-PCF [15]. Collapsing enlarges the mode field at the interface of the PM-PCF so as to match the mode field of the single-mode fiber (SMF). The Sagnac interferometer is laid in an open metal box and the box is placed inside a sealed air tank. The tank is connected to an air compressor with adjustable air pressure that was measured with a pressure meter. The input and output ends of the Sagnac interferometer are placed outside the air tank. When a broadband light source (amplified spontaneous emission source with pumped erbium-doped fiber) is connected to the input, an interference output, as shown in Fig. 2, can be observed. By measuring the wavelength shift of one of the transmission minimums with an optical spectrum analyzer (OSA), the applied pressure to the PM-PCF can be determined.

In the fiber loop, the two counterpropagating lights split by the 3 dB SMF coupler interfere again at the coupler and the resulting spectrum is determined by the relative phase difference introduced to the two orthogonal guided modes mainly by the PM-PCF. Ignoring the loss of the Sagnac loop, the transmission spectrum of the fiber loop is approximately a periodic function of the wavelength and is given by

$$T = [1 - \cos(\delta)]/2. \quad (1)$$

The total phase difference  $\delta$  introduced by the PM-PCF can be expressed as

$$\delta = \delta_0 + \delta_P, \quad (2)$$

where  $\delta_0$  and  $\delta_P$  are the phase differences due to the intrinsic and pressure-induced birefringence over the length  $L$  of the PM-PCF and are given by

$$\delta_0 = \frac{2\pi \cdot B \cdot L}{\lambda}, \quad (3)$$

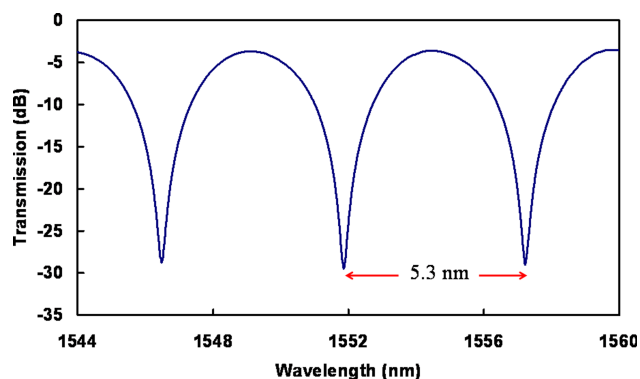


Fig. 2. (Color online) Transmission spectrum of the PM-PCF based Sagnac interferometer.

$$\delta_P = \frac{2\pi \cdot (K_P \Delta P) \cdot L}{\lambda} \quad (4)$$

$B = n_s - n_f$  is the birefringence of the PM-PCF;  $n_s$  and  $n_f$  are effective refractive indices of the PM-PCF at the slow and fast axes, respectively.  $\Delta P$  is the applied pressure and the birefringence-pressure coefficient of PM-PCF can be described as [10]

$$K_P = \frac{\partial n_s}{\partial P} - \frac{\partial n_f}{\partial P} \quad (5)$$

The spacing  $S$  between two adjacent transmission minima can be approximated by

$$S = \lambda^2 / (B \cdot L) \quad (6)$$

The pressure-induced wavelength shift of the transmission minimum is  $\Delta\lambda = S \cdot \delta_P / 2\pi$ . Thus, the relationship between wavelength shift and applied pressure can be obtained by

$$\Delta\lambda = \left( \frac{K_P \cdot \lambda}{B} \right) \cdot \Delta P \quad (7)$$

Equation (7) shows that for a small wavelength shift the spectral shift is linearly proportional to the applied pressure.

### 3. Experimental Results and Discussions

Figure 2 shows the transmission spectrum of the PM-PCF-based Sagnac interferometer at atmospheric pressure, i.e., at zero applied pressure. The spacing between two adjacent transmission minima is  $\sim 5.3$  nm and an extinction ratio of better than 20 dB was achieved. The intrinsic birefringence of the PM-PCF used in our experiment is  $7.8 \times 10^{-4}$  at 1550 nm.

The air compressor is initially at one atmospheric pressure (about 0.1 MPa). In our experiment, we can increase air pressure up to 0.3 MPa; thus, the maximum pressure that can be applied to the PM-PCF-based Sagnac interferometer sensor is  $\sim 0.4$  MPa. At one atmospheric pressure one of the transmission minima occurs at 1551.86 nm and shifts to a longer wavelength with applied pressure. When the applied pressure was increased by 0.3 MPa, a 1.04 nm wavelength shift of the transmission minimum was measured, as shown in Fig. 3. Figure 4 shows the experimental data of the wavelength–pressure variation and the linear curve fitting. The measured wavelength–pressure coefficient is 3.42 nm/MPa with a good  $R^2$  value of 0.999, which agrees well with our theoretical prediction. From Eq. (7), the birefringence–pressure coefficient is  $\sim 1.7 \times 10^{-6}$  MPa $^{-1}$ . The resolution of the pressure measurement is  $\sim 2.9$  kPa when using an OSA with a 10 pm wavelength resolution. Because of the limitations of our equipment, we have not studied the performance of this pressure sensor for high pressure at this stage. However, we found that the PM-PCF can stand pres-

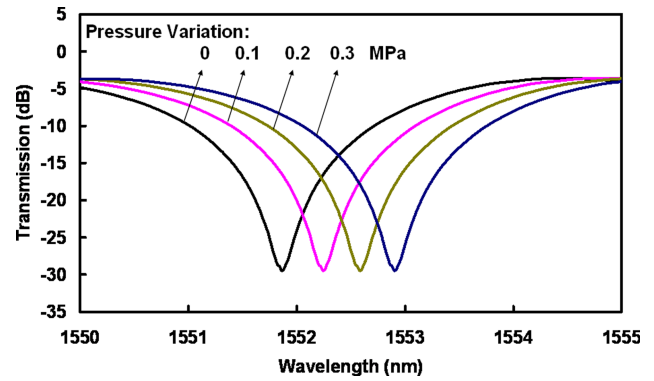


Fig. 3. (Color online) Measured transmission spectra under different pressures.

sure of 10 MPa without damage to its structure. This part of the work is ongoing and will be reported in our further studies.

Although the length of PM-PCF used in our experiment is 58.4 cm, it is important to note that the PM-PCF can be coiled into a very small diameter circle with virtually no additional bending loss so that a compact pressure sensor design can be achieved. The induced bending loss by coiling the PM-PCF fiber into 10 turns of a 5 mm diameter circle, shown in the inset of Fig. 4, is measured to be less than 0.01 dB with a power meter (FSM-8210, ILX Lightwave Corporation). The exceptionally low bending loss will simplify sensor design and packaging and fulfills the strict requirements of some applications where small size is needed, such as in down-hole oil well applications. To investigate the effects of coiling, we have studied two extreme cases in which the PM-PCF was wound with its fast axis and then its slow axis on the same plane of the coil. There were no measurable changes for either the birefringence or the wavelength–pressure coefficient when the fiber was coiled into 15 and 6 mm diameter circles with both of the orientations coiling. The coiling of the PM-PCF into small diameter circles makes the entire sensor very compact and could reduce any unwanted environmental distortions, such as vibrations.

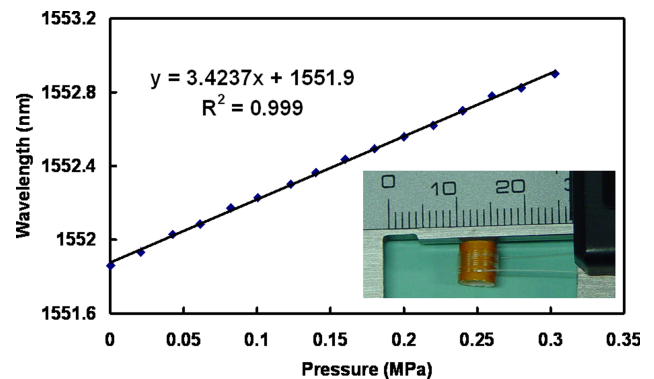


Fig. 4. (Color online) Wavelength shift of the transmission minimum at 1551.86 nm against applied pressure with variation up to 0.3 MPa based on one atmospheric pressure.

The wavelength–pressure coefficient is independent of the length of the PM-PCF, as described in Eq. (7). Figure 5 shows the wavelength–pressure coefficients are 3.46 and 3.43 nm/MPa for PM-PCFs with lengths of 40 and 79.6 cm, respectively. After comparing the two wavelength–pressure coefficients with that of the pressure sensor with a 58.4 cm PM-PCF (Fig. 4), we observed that the wavelength–pressure coefficient is constant around 1550 nm; this agrees well with our theoretical prediction. However, the length of the PM-PCF cannot be reduced too much because this would result in broad attenuation peaks in the transmission spectrum and that would reduce the reading accuracy of the transmission minimums.

Temperature sensitivity of the proposed pressure sensor is also investigated by placing the sensor into an oven and varying its temperature. Figure 6 shows the wavelength shift of a transmission minimum versus temperature linearly with a good  $R^2$  value of 0.9984. The measured temperature coefficient is  $-2.2 \text{ pm}/^\circ\text{C}$ , which is much smaller than the  $10 \text{ pm}/^\circ\text{C}$  of fiber Bragg grating. The temperature may be neglected for applications that operate over a normal temperature variation range.

Based on the small size, the high wavelength–pressure coefficient, the reduced temperature sensitivity characteristic, and other intrinsic advantages of fiber optic sensors, such as light weight and electromagnetically passive operation, the proposed pressure sensor is a promising candidate for pressure sensing even in harsh environments. Considering the whole pressure sensing system, we can also replace the light source with laser and use a photodiode for intensity detection at the sensing signal receiving end. Since the power fluctuation is very small even when the PM-PCF is bent, intensity detection is practical for real applications. Because of the compact size of the laser and photodiode, the entire system can be made into a very portable system. Furthermore, the use of intensity detection instead of wavelength measurement would greatly enhance interrogation speed and consequently makes the system much more attractive.

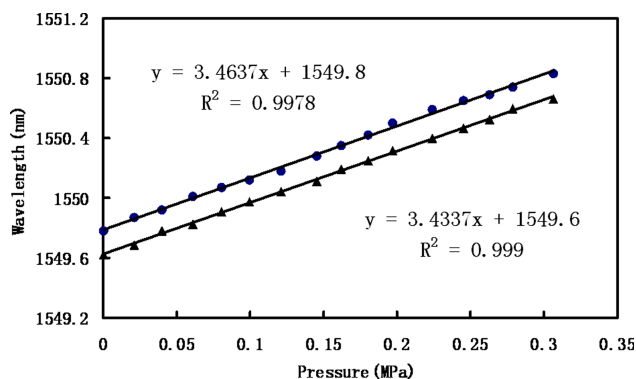


Fig. 5. (Color online) Wavelength shift of the transmission minimum against applied pressure for PM-PCFs with length of 40 (circles) and 79.6 cm (triangles); the wavelength–pressure coefficients are 3.46 and 3.43 nm/MPa, respectively.

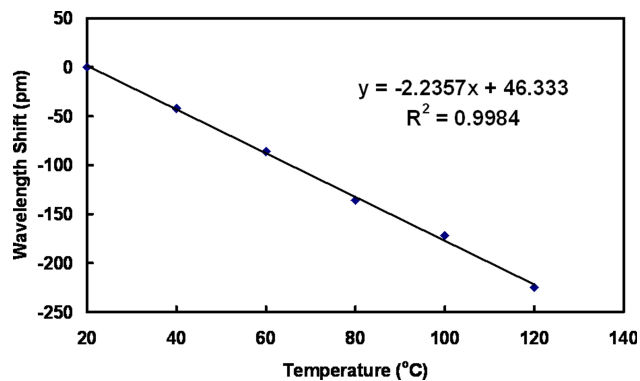


Fig. 6. (Color online) Wavelength shift of the transmission minimum at 1551.86 nm against temperature.

#### 4. Conclusion

A novel fiber Sagnac interferometer pressure sensor realized by using a PM-PCF as the sensing element has been proposed and demonstrated. Experimental results and simplified theoretical analysis of the pressure sensor have been presented. The sensitivity of the pressure sensor is 3.42 nm/MPa. The proposed pressure sensor exhibits the advantages of high sensitivity, compact size, low temperature sensitivity, and is potentially low cost.

The authors thank Dr. Limin Xiao and Dr. S. Y. Liu for fruitful discussions and timely help. This work was supported in part by the Hong Kong Polytechnic University under project G-U263 and in part by the Central Research Grant of the Hong Kong Polytechnic University under project G-YX77.

#### References

1. V. Vali and R. W. Shorthill, "Fiber ring interferometer," *Appl. Opt.* **15**, 1099–1103 (1976).
2. S. Knudsen and K. Blotekjaer, "An ultrasonic fiber-optic hydrophone incorporating a push–pull transducer in a Sagnac interferometer," *J. Lightwave Technol.* **12**, 1696–1700 (1994).
3. A. N. Starodumov, L. A. Zenteno, D. Monzon, and E. De La Rose, "Fiber Sagnac interferometer temperature sensor," *Appl. Phys. Lett.* **70**, 19–21 (1997).
4. E. De La Rose, L. A. Zenteno, A. N. Starodumov, and D. Monzon, "All-fiber absolute temperature sensor using an unbalanced high-birefringence Sagnac loop," *Opt. Lett.* **22**, 481–483 (1997).
5. Y. J. Song, L. Zhan, S. Hu, Q. H. Ye, and Y. X. Xia, "Tunable multiwavelength Brillouin–erbium fiber laser with a polarization-maintaining fiber Sagnac loop filter," *IEEE Photon. Technol. Lett.* **16**, 2015–2017 (2004).
6. M. Campbell, G. Zheng, A. S. Holmes-Smith, and P. A. Wallace, "A frequency-modulated continuous wave birefringent fibre-optic strain sensor based on a Sagnac ring configuration," *Meas. Sci. Technol.* **10**, 218–224 (1999).
7. Y. Liu, B. Liu, X. Feng, W. Zhang, G. Zhou, S. Yuan, G. Kai, and X. Dong, "High-birefringence fiber loop mirrors and their applications as sensors," *Appl. Opt.* **44**, 2382–2390 (2005).
8. G. Kakarantzas, A. Ortigosa-Blanch, T. A. Birks, P. St. Russell, L. Farr, F. Couny, and B. J. Mangan, "Structural rocking filters in highly birefringent photonic crystal fiber," *Opt. Lett.* **28**, 158–160 (2003).

9. X. Dong, H. Y. Tam, and P. Shum, "Temperature-insensitive strain sensor with polarization-maintaining photonic crystal fiber based Sagnac interferometer," *Appl. Phys. Lett.* **90**, 151113 (2007).
10. H. K. Gahir and D. Khanna, "Design and development of a temperature-compensated fiber optic polarimetric pressure sensor based on photonic crystal fiber at 1550 nm," *Appl. Opt.* **46**, 1184–1189 (2007).
11. C.-L. Zhao, X. Yang, C. Lu, W. Jin, and M. S. Demokan, "Temperature-insensitive interferometer using a highly birefringent photonic crystal fiber loop mirror," *IEEE Photon. Technol. Lett.* **16**, 2535–2537 (2004).
12. D.-H. Kim and J. U. Kang, "Sagnac loop interferometer based on polarization maintaining photonic crystal fiber with reduced temperature sensitivity," *Opt. Express* **12**, 4490–4495 (2004).
13. T. P. Hansen, J. Broeng, S. E. B. Libori, E. Knudsen, A. Bjarklev, J. R. Jensen, and H. Simonsen, "Highly birefringent index-guiding photonic crystal fibers," *IEEE Photon. Technol. Lett.* **13**, 588–590 (2001).
14. Y. Zhang, D. Feng, Z. Liu, Z. Guo, X. Dong, K. S. Chiang, and B. C. B. Chu, "High-sensitivity pressure sensor using a shielded polymer-coated fiber Bragg grating," *IEEE Photon. Technol. Lett.* **13**, 618–619 (2001).
15. L. Xiao, W. Jin, and M. S. Demokan, "Fusion splicing small-core photonic crystal fibers and single-mode fibers by repeated arc discharges," *Opt. Lett.* **32**, 115–117 (2007).